JARO (2014)
DOI: 10.1007/s10162-014-0459-7

JARO
Journal of the Association for Research in Otolaryngology

Research Article

Hearing Loss is an Early Consequence of *Npc1* Gene Deletion in the Mouse Model of Niemann–Pick Disease, Type C

Kelly A. King,[1] Sandra Gordon-Salant,[2] Karen S. Pawlowski,[5] Anna M. Taylor,[6] Andrew J. Griffith,[1] Ari Houser,[3] Kiyoto Kurima,[1] Christopher A. Wassif,[4] Charles G. Wright,[5] Forbes D. Porter,[4] Joyce J. Repa,[6,7] and Carmen C. Brewer[1]

[1]*National Institute on Deafness and Other Communication Disorders, National Institutes of Health, Bethesda, MD 20892, USA*

[2]*Department of Hearing and Speech Sciences, University of Maryland College Park, College Park, MD 20742, USA*

[3]*Department of Human Development and Quantitative Methodology, University of Maryland College Park, College Park, MD 20742, USA*

[4]*Eunice Kennedy Shriver National Institute of Child Health and Human Development, National Institutes of Health, Bethesda, MD 20892, USA*

[5]*Department of Otolaryngology, UT Southwestern Medical Center, Dallas, TX 75390, USA*

[6]*Department of Physiology, UT Southwestern Medical Center, Dallas, TX 75390, USA*

[7]*Department of Internal Medicine, UT Southwestern Medical Center, Dallas, TX 75390, USA*

Received: 31 December 2012; Accepted: 24 April 2014

ABSTRACT

Niemann–Pick disease, type C1 (NPC1) is a rare lysosomal lipidosis that is most often the result of biallelic mutations in *NPC1*, and is characterized by a fatal neurological degeneration. The pathophysiology is complex, and the natural history of the disease is poorly understood. Recent findings from patients with NPC1 and hearing loss suggest that multiple steps along the auditory pathway are affected. The current study was undertaken to determine the auditory phenotype in the $Npc1^{nih}$ mutant mouse model, to extend analyses to histologic evaluation of the inner ear, and to compare our findings to those reported from human patients. Auditory testing revealed a progressive high-frequency hearing loss in $Npc1^{-/-}$ mice that is present as early as postnatal day 20 (P20), well before the onset of overt neurological symptoms, with evidence of abnormalities involving the cochlea, auditory nerve, and brainstem auditory centers. Distortion product otoacoustic emission amplitude and auditory brainstem response latency data provided evidence for a disruption in maturational development of the auditory system in $Npc1^{-/-}$ mice. Anatomical study demonstrated accumulation of lysosomes in neurons, hair cells, and supporting cells of the inner ear in P30 $Npc1^{-/-}$ mice, as well as increased numbers of inclusion bodies, myelin figures, and swollen nerve endings in older (P50–P70) mutant animals. These findings add unique perspective to the pathophysiology of NPC disease and suggest that hearing loss is an early and sensitive marker of disease progression.

Keywords: NPC, hearing, auditory maturation, auditory brainstem response (ABR)

INTRODUCTION

Niemann–Pick disease, type C1 (NPC1) is a rare (1:120,000–150,000) autosomal recessive disorder of lipid metabolism that typically affects children and is characterized by hepatic dysfunction in the neonatal/infantile period and subsequent neurological decline.

Correspondence to: Carmen C. Brewer · National Institute on Deafness and Other Communication Disorders · National Institutes of Health · Bethesda, MD 20892, USA. Telephone: +301-496-5294; email: brewerc@nidcd.nih.gov

Published online: 17 May 2014

It is a clinically and genetically complex and heterogeneous disease that most often results from biallelic mutations in *NPC1*. The principal metabolic defect alters cholesterol trafficking from lysosomes (Liscum and Faust 1987; Liscum et al. 1989) and creates an excess accumulation of unesterified cholesterol and other lipid moieties within cells and tissues throughout the body. There is preferential damage to neurons (Ordonez et al. 2012) and areas with high concentrations of lipids in the brain, such as myelin and neural plasma membranes (Vincent et al. 2003). Onset of neurological symptoms classically begins in the late-infantile and juvenile years; however, age of presentation can range from the perinatal period to adulthood. The persistent and widespread neurodegeneration is fatal in all cases and, currently, there is no definitively effective intervention.

Early evidence suggested the auditory system is affected by NPC1 (Fink et al. 1989; Pikus 1991; Garver et al. 2007), although it has likely been an underreported manifestation given the difficulty in obtaining behavioral audiological assessments from a pediatric, neurologically compromised population. Current data, including behavioral measures, auditory brainstem responses and distortion product otoacoustic emissions, obtained from a large cohort of humans with NPC1 (King et al. 2014) confirm a functionally significant, often high-frequency, progressive auditory phenotype with evidence for dysfunction in the peripheral and central auditory pathways.

Homozygous mutant *Npc1*^{nih} mice on a Balb/c background strain (Loftus et al. 1997) lack functional NPC1 protein and present with comparable molecular, anatomical, and biochemical phenotypes to humans with Niemann–Pick C disease. Affected animals show age-related Purkinje cell loss, demyelination in the corpus callosum (German et al. 2001; Weintraub et al. 1992), widespread cortical effects (Ong et al. 2001), and evidence for a global reduction in white matter tracts (Ory 2000). Overt neurological symptoms (e.g., visible ataxia) may not manifest until postnatal day 45 (P45) or later, although retarded growth and neuromuscular dysfunction are present at 5 weeks (Võikar et al. 2002; Li et al. 2005).

Therapeutic trials with 2-hydroxypropyl-ß-cyclodextrin (HP-ß-CD) have been conducted in feline and mouse models of NPC disease, and are currently being extended to humans with this genetic disorder. While HP-ß-CD has shown promising results in animal models by increasing the lifespan and ameliorating cerebellar neurodegeneration, profound and irreversible hearing loss has been observed in diseased and control cats treated with the drug (Ward et al. 2010). This presents a need to expand understanding of the auditory phenotype of NPC1 across species. Auditory function beyond the acoustic startle has not been reported in the *Npc1*^{nih} mouse; however, brainstem histology identified changes in central auditory system nuclei in mutant mice, including lower neural density in the ventral cochlear nucleus and a proliferation of astrocytes in the inferior colliculus and medial geniculate nuclei (Luan et al. 2008).

We present the first physiologic, electrophysiologic, and histologic longitudinal data from the cochlea and auditory nerve of the *Npc1*^{nih} mouse, which provide a unique perspective on the pathological processes associated with *NPC1* mutations, and support the auditory system in this species as a useful marker for disease status, progression, and potentially therapeutic efficacy.

METHODS

Animals

Maintenance and care of the mice followed the *Guide for the Care and Use of Laboratory Animals* (Institute for Laboratory Animal Research, Committee for the Update of the Guide for the Care and Use of Laboratory Animals 2011). The combined National Institute of Neurological Disorders and Stroke and National Institute on Deafness and Other Communication Disorders Animal Care and Use Committee approved studies performed at NIH (AJG) and the Institutional Animal Care and Use Committee approved mouse experiments performed at UT Southwestern Medical Center at Dallas (JJR). Homozygous *Npc1*$^{+/+}$, heterozygous *Npc1*$^{+/-}$, and homozygous *Npc1*$^{-/-}$ mice were obtained from matings of heterozygous *Npc1*$^{+/-}$ male and female mice (BALB/cNctr-*Npc1*^{m1N}/J strain). Genomic DNA was prepared from tail clip or ear punch biopsies, and genotypes were determined by PCR using forward primer (GGTGCTGGACAGCCAAGTA) and reverse primer (GATGGTCTGTTCTCCCATG) as described (Loftus et al. 1997).

For auditory testing, 20 mice from each experimental (genotype) group were evaluated starting at P20 every 5 days until P65, for a total of 60 mice with 10 longitudinal data points. Given the neurodegenerative phenotype, endpoint criteria for euthanasia were established (15 % loss of total body weight or an observation that the animal was moribund, cachectic, or unable to obtain food or water). All animals survived until P65, although very few survived long after, thus establishing the experimental lifespan. For histologic evaluation, both ears from five to ten animals of each genotype were prepared at P30, P50, and P70.

Auditory Testing

Animals were anesthetized using a combined cocktail of ketamine and dexdormitor (56 mg/kg bodyweight and 0.375 mg/kg bodyweight, respectively), administered via subcutaneous injection. Total dosage of anesthesia was weight dependent, and neither of these drugs is known to affect auditory function in this species. Animals were placed on a heating pad, and their temperature was maintained at 37 °C via a rectal thermometer throughout testing in a sound-shielded test booth. The examiner was blind to the genotype, although in older mice, mutants could be identified based on an overt neurological phenotype.

Distortion product otoacoustic emissions (DPOAE) were recorded with an ER-10C (Etymotic Research, Inc., Elk Grove Village, IL) speaker-probe assembly using the DP2000 DPOAE measurement system, version 3.0 (Starkey Laboratories, Eden Prairie, MN). The speaker-probe assembly was placed in the external auditory canal of the animal. Two tones (f_1 and f_2, $f_2>f_1$) were presented at f_1=65 dB SPL and f_2=55 dB SPL. Calibration of the two tones took place in situ. The tones were varied in one twelfth octave steps from f_2=5,297 to 10,641 Hz, based on the frequency limitations of the speaker-probe assembly, with a constant frequency ratio (f_2/f_1) of 1.2. DPOAE amplitudes were recorded from both ears of each animal and then the amplitudes were averaged, along with the noise floors.

Following DPOAE collection, ABRs were obtained from a single ear (counterbalanced between animals, and maintained throughout longitudinal testing). Three subdermal needle electrodes (forehead and both mastoids) were placed for recording. ABR stimuli were generated with the auditory-evoked Intelligent Hearing Systems (Miami, FL) software and produced through a high-frequency (HFT9911-20-0035), closed-field transducer. ABR thresholds were obtained using a negative polarity (rarefaction) click stimulus, as well as 8, 16, and 32 kHz tone pips, presented at a rate of 21/s. Duration of the stimulus was 47 and 1,000 μs for click and tone-pip stimuli, respectively. Prior to beginning threshold searches, a response to a high intensity (e.g., 110 dB SPL) suprathreshold stimulus was collected and used to determine absolute and interpeak latencies, as well as waveform amplitude. The same number of artifact-free sweeps (1,024) was collected to obtain the suprathreshold response at every test session on each animal.

ABR threshold search began with a 110-dB SPL signal for click, 8 and 16 kHz stimuli, and a 100-dB SPL signal for the 32 kHz stimulus (based on equipment limitations). The intensity was then decreased in 10 dB steps until no response was obtained, followed by 5 dB steps at lower intensities near threshold. Threshold was defined as the lowest intensity level (dB SPL) that elicited a time-locked and replicable response waveform above the noise floor. The noise floor was evaluated via a control run using a 0-dB SPL stimulus. A minimum of 400 artifact-free sweeps were obtained for each waveform. Following collection of suprathreshold data and determination of thresholds for click and tone-pip stimuli, the effects of sedation were reversed using an antecedent, and the animal was returned to a recovery cage.

Histology

Light and Transmission Electron Microscopy

Mice were killed under deep anesthesia (ketamine/xylazine/acepromazine), and both temporal bones were quickly removed from the skull. Middle and inner ears were opened bilaterally and perfused with, then fixed in, 2.5 % glutaraldehyde in 0.1 M sodium phosphate buffer (PBS; pH 7.4; Sigma Aldridge, St. Louis) for 5–7 days at 4 °C. Tissues were then rinsed in PBS. Several embedding methods were used to screen for pathological changes in the tissue. Tissues used for screening of the entire inner ear were embedded in JB-4 (Electron Microscopy Sciences, Hatfield PA). The embedding process was as follows: fixed tissue was decalcified in 0.35 M EDTA at room temperature for at least 7 days with constant agitation. Tissues were then rinsed in PBS, dehydrated in a series of ethanol solutions of increasing concentration, and embedded in JB-4. For closer examination at the ultramicroscopic level, glutaraldehyde-fixed tissue was stained in 1 % osmium tetroxide in PBS, rinsed in PBS and decalcified, rinsed in PBS, dehydrated in a series of ethanol solutions, and embedded in Embed-812 (Electron Microscopy Sciences, Hatfield PA). Tissues embedded in either compound were serially sectioned at a thickness of 4–5 μm, mounting every third section. The sectioning was performed in a plane approximately parallel to the long axis of the modiolus. Sections were stained with toluidine blue, coverslipped, and examined under an Olympus BH2 compound microscope (Olympus, Center Valley, PA). For transmission electron microscopy, ultrathin sections were taken in the same orientation as the light microscopy sections. Sections were stained with lead citrate and uranyl acetate and examined using a JEOL 1200EX transmission electron microscope made available by the UT Southwestern Electron Microscopy Core.

Post hoc quantification of elongation of the major axis of the spiral ganglion cell soma was performed on sections from JB-4 embedded P30 ears, using images

from ears of three NPC and three control mice. Analysis included only mid-modiolar sections in which the organ of Corti was cross-sectioned and the majority of the nerves within Rosenthal's canal were longitudinally sectioned. The area of analysis was restricted to spiral ganglion in the region ½ to ¾ turn apical from the round window membrane. Images were taken from 3-4 sections of each ear, with the sections spaced approximately 30 μm apart. Images were randomized, and randomly placed line-grids were projected across each photo. Only cell somata that touched the line intersections were counted. The ratio of the lengths of the major versus minor axes of the cells was obtained for cells in which the nucleus and nucleoli were present. Two examiners blinded to the condition of each image measured a total of 169 cells from NPC mice and 203 cells from control mice utilizing Image J software. Statistical analysis was performed on the population of cells from NPC and control mice utilizing Student's *t* test.

Filipin Staining

Mice were placed under deep anesthesia (ketamine/xylazine) and subjected to transcardial perfusion with 4 % formalin. Both temporal bones were quickly removed, the middle and inner ears opened and immersed in formalin for 7 days, then rinsed in PBS. The inner ear was dissected in PBS, without decalcification, and incubated with filipin (final concentration of 50 μg/ml in PBS; Sigma, F-9765) for 1.5 h with gentle rotation and shielding from light. The tissue pieces were washed 3 times with PBS, then mounted on glass slides and imaged using a DVRT Deltavision Deconvolution Microscope (inverted wide-field epifluorescence microscope) made available by the UT Southwestern Live Cell Imaging Core. Filipin signal was acquired using the following UV settings: excitation, BP 360/40; emission, BP 470/40; and dichroic mirror, 400, as kindly recommended by Fred Maxfield (Weill Cornell Medical College). Exposure times were the same for wild type and NPC1$^{-/-}$ samples (0.5 s). For each specimen, Z-stacks of 60 images were acquired with a step size of 0.15 μm. Z-stacks were deconvolved using Autoquant software (Media Cybernetics). Images in Figure 6 are maximum-intensity projections of the deconvolved Z-stacks using the Image>Stacks>Z Project function in ImageJ.

Statistical Analysis

Data were maintained and analyzed using Microsoft Excel, the Statistical Package for Social Sciences Software (SPSS, v15) and the SAS (SAS, v9.1) software packages. For all statistical analyses, α=0.05.

To evaluate neural and cochlear function, change over time, and effect of disease within gender, DPOAE (averaged between the right and left ears) and ABR data were analyzed with the Proc MIXED procedure in SAS 9.1 using a repeated measures model with autoregressive correlation matrix structure (Crowder and Hand 1990) instead of the more commonly used compound symmetry model. The autoregressive structure postulates that the correlation is stronger between time points that are closer together and weaker between time points that are farther apart. Fit statistics confirmed the logical assumption that the autoregressive model was more appropriate for this dataset.

DPOAE amplitude and ABR (click and tone pip) threshold, suprathreshold peak latency (absolute and interpeak) and suprathreshold peak amplitude were evaluated in separate analyses. For all dependent variables, the assumed model was:

$$Y = \text{intercept} + \text{gender} + \text{genotype(homozygous/non-homozygous)} + \text{time} + \text{all interactions}$$

Preliminary analyses revealed no significant differences in measures of hearing (DPOAE amplitude, ABR threshold, latency, and amplitude) between *Npc1^{nih}* heterozygous carriers (+/−) and control (+/+) littermates. Therefore, data from these two groups were pooled to establish a larger control data set (*Npc1^{nih}* +/−, +/+) and increase statistical power.

RESULTS

Npc1^{nih} Mutant Mice Exhibit Hearing Loss as Early as Postnatal Day 20 that Deteriorates Across the Lifespan

Repeated measures modeling revealed that homozygous mutant *Npc1^{nih}* mice have significantly (p<0.05) elevated ABR thresholds at P20 compared with heterozygous (*Npc1^{nih}* +/−) and control (*Npc1^{nih}* +/+) animals at 16 and 32 kHz (Fig. 1A) and by P65 this pattern is present for all test stimuli (Fig. 1B). Data from our control animals (BALB/c-*Npc1^{nih}* +/−, +/+) indicate that age-related decline in high-frequency hearing (32 kHz, Fig. 2D) can begin earlier than previously reported in this background strain (Willott et al. 1998).

Npc1^{nih} homozygous mutant mice exhibited significant progressive elevations in ABR thresholds at rates of 0.32, 0.4, and 0.7 dB every 5 days for click, 8 and 16 kHz stimuli, respectively, with no significant change in the hearing of control animals (Fig. 2A–C). Repeated measures modeling identified a significantly (p<0.02) poorer ABR threshold

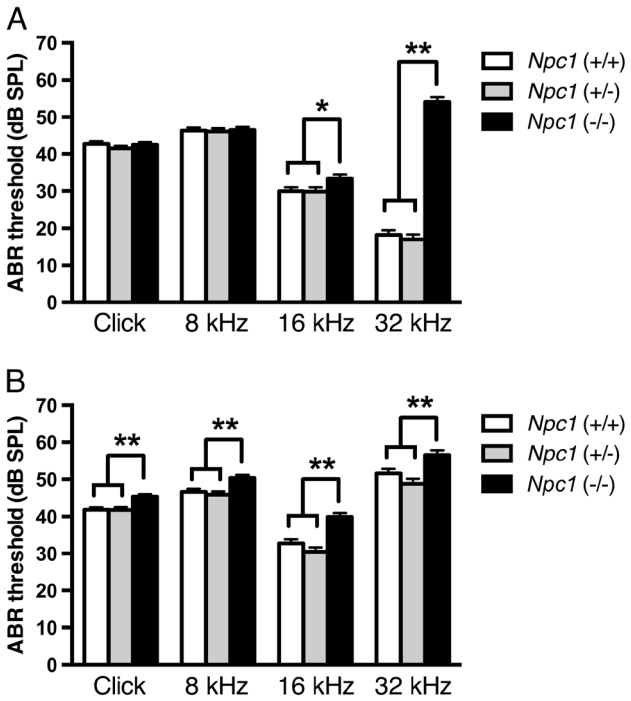

FIG. 1. Estimated average ABR thresholds from left and right ears (counterbalanced between animals) and standard error of the mean from repeated measures modeling for control (+/+), heterozygous (+/−), and homozygous (−/−) *Npc1*^{nih} mice at P20 (**A**) and P65 (**B**). Differences between control and heterozygous groups are not statistically significant at any frequency. *p<0.05; **p<0.001.

in *Npc1*^{nih} homozygous mutant mice compared with controls for click and 8 kHz stimuli by P35. At 32 kHz, control animals exhibited a significant elevation in ABR threshold of 3.6 dB every five days, while thresholds of *Npc1*^{nih} homozygous mutant animals remained stable (Fig. 2D). Despite the progressive elevation in 32 kHz thresholds for control animals, *Npc1*^{nih} homozygous mutant mice had significantly poorer ABR thresholds at 32 kHz across the entire experimental lifespan.

Otoacoustic Emissions Support a Functional Cochlear Lesion and Suggest Disruption in Sensory Maturation in the Npc1^{nih} (−/−) Mouse

To localize a functional site of lesion for the elevated ABR thresholds observed in *Npc1*^{nih} homozygous mutant mice, $2f_1$–f_2 DPOAE amplitudes were analyzed longitudinally in *Npc1*^{nih} mutant and control (+/−, +/+) animals from 5,297 to 10,641 Hz. DPOAEs are believed to reflect active biological processes within the cochlea, specifically electromotile properties of the outer hair cells. Both *Npc1*^{nih} homozygous mutant mice and control animals displayed relatively robust signal-to-noise ratios (SNR) across the experimental lifespan (Fig. 3A versus B). *Npc1*^{nih} control (+/−, +/+) animals displayed a significant increase in DPOAE amplitude across f_2 test frequencies at all time points during the experimental lifespan (Table 1, DPOAE amplitude progression/5 days). However, DPOAE amplitudes in homozygous mutant *Npc1*^{nih} mice only increased in amplitude for the lower test frequencies (5,297–6,891 Hz), and not to the degree observed in control animals (Table 1, DPOAE amplitude progression/5 days). No increase in emission amplitude was observed in the higher test frequencies for these mice. At P20, *Npc1*^{nih} homozygous mutant animals had significantly (p<0.01) lower DPOAE amplitudes compared with control animals at all but two test frequencies (7,547 and 10,641 Hz) (Table 1, P20 DPOAE amplitude). This significant difference persisted across the experimental lifespan such that at P65, homozygous mutant *Npc1*^{nih} mice continued to have lower $2f_1$-f_2 distortion product amplitudes at all test frequencies (Table 1, P65 DPOAE amplitude).

ABR Latencies Implicate Maturational Disruption of Neural Auditory Pathways in Npc1^{nih} (−/−) Mice

To evaluate the functional integrity of the auditory nerve and auditory brainstem tracts, ABRs were measured in response to high-intensity stimuli and absolute (I, II, III, IV, and V) and interpeak (I–III, III–V, and I–V) latency data from the component peaks of the waveform were analyzed. For the click stimulus (Table 2, P20 Latency), there were no significant differences in absolute or interpeak latency at P20 between *Npc1*^{nih} homozygous mutant mice and control (+/−, +/+) animals. Latency data from mutant mice did not change significantly over time, with the exception of a slight increase (0.005 ms/5 days) in the absolute latency of wave I. Conversely, control animals exhibited a significant decrease in latency over time across all component peaks of the waveform. In general, the effect was greater for later-occurring waves (Table 2; Fig. 4).

A similar pattern as the one observed with a click stimulus was seen for the tone-pip ABR stimuli (data not shown). Few differences in latency existed between control (+/−, +/+) and mutant (−/−) *Npc1*^{nih} animals at P20, and of those (n=6) all but one (wave II, 8 kHz) revealed that *Npc1*^{nih} mutant mice had prolonged latencies compared with control animals. The more robust finding, however, was that for all ABR stimuli, control animals underwent a significant decrease in latency across the experimental lifespan at almost every component of the waveform. As with the click stimulus, the effect was generally greater for later-occurring waves. *Npc1*^{nih} homozygous mutant mice, however, exhibited far fewer significant changes

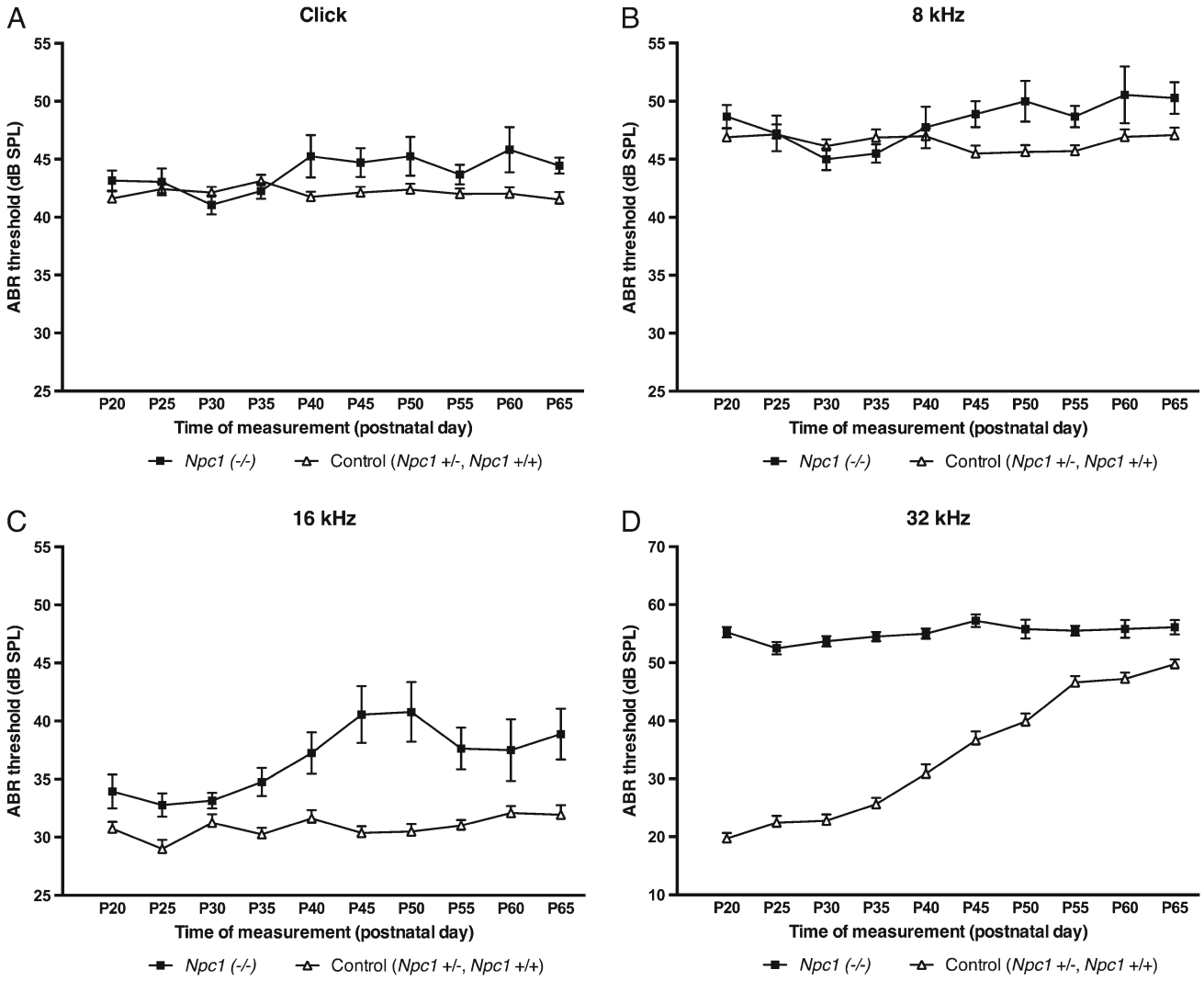

FIG. 2. Mean (SEM) ABR threshold progression for click (**A**), 8 k Hz (**B**), 16 kHz (**C**), and 32 kHz (**D**) stimuli for *Npc1*^{nih} homozygous mutant (−/−) and control (+/−, +/+) mice.

in latency over this time period, and most changes involved a prolongation in the absolute latency of early waves, with a concomitant decrease in interpeak latencies. These progressive shifts across the experimental lifespan culminated in *Npc1*^{nih} homozygous mutant mice having significantly longer latencies than control animals for all but three (29/32) ABR waveform components at P65 (Table 2 for click stimuli; data not shown for tone-pip stimuli).

ABR amplitudes (data not shown) revealed no clear effect of disease for either the click or 8 kHz stimuli. Smaller amplitudes were noted for 16 and 32 kHz stimuli in homozygous mutant *Npc1*^{nih} mice compared with controls (+/−, +/+), primarily for the early ABR peaks (I, II, and III), which is consistent with the early-onset hearing loss observed at these frequencies.

Gender differences in auditory function were not significant in most analyses (data not shown).

Histological Changes Indicate Cholesterol Accumulation Occurs in Cochlear Tissue by P30

Imaging of plastic embedded toluidine blue-stained cochlear tissue revealed cellular changes in the cochlear duct of homozygous mutant *Npc1*^{nih} mice compared with controls (*Npc1* +/+) that were apparent at the light microscopic level by P30. The changes most consistently seen at this time were accumulation of lysosomes or inclusion bodies in the spiral ganglion cells that appeared to cause expansion of the cell soma at both poles and accumulation of inclusion bodies within the supporting cells of the organ of Corti and stria vascularis. Determination of the ratio of the lengths of the major versus minor axes of the spiral ganglion cell soma revealed a significant difference in axis ratio for the population of *Npc1*^{nih} (−/−) versus control (*Npc1*^{nih} +/+) spiral ganglion somata (p=0.004). The mean ratio for somata of

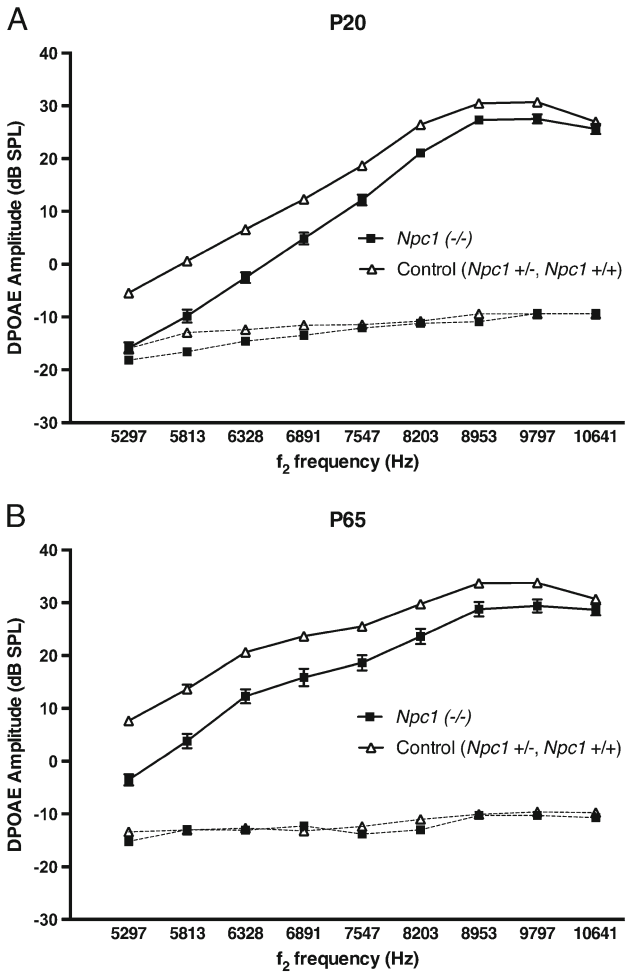

FIG. 3. Mean (SEM) DPOAE amplitude (*solid lines*) from left and right ears for *Npc1*^{nih} homozygous mutant (−/−) and control (+/−, +/+) mice as a function of f_2 frequency at P20 (**A**) and P65 (**B**). *Dashed lines* represent DPOAE noise floor.

Npc1^{nih} (−/−) cells was 1.81 (±0.44 (standard deviation), n=169) versus 1.66 (±0.38, n=203) for control. By P30, swelling could also be seen in the afferent and efferent fibers within the organ of Corti (Fig. 5), which become more apparent by P50 and P70. Similar changes have been reported for CNS neurons in NPC disease (Walkley and Suzuki 2004).

Filipin staining of cochlear tissue from P50 homozygous mutant *Npc1*$^{nih-/-}$ mice revealed bright punctate staining within cells of the stria vascularis and the organ of Corti (Fig. 6). Filipin, a fluorescent probe that forms a complex specifically with unesterified cholesterol, reveals the lysosomal sterol accumulation that is a hallmark of this disease (Patterson et al. 2001). Lysosomal sterol/filipin was only observed in *Npc1*$^{nih-/-}$ mice and was readily apparent in the intermediate cell layer of the stria vascularis and supporting cells of the organ of Corti, although some staining of vesicles was also seen in inner and outer hair cells. Punctate filipin staining was not detected in

TABLE 1

Results of repeated measures modeling for DPOAE amplitude (dB SPL) at P20 and P65 and DPOAE amplitude progression (dB)

	P20 DPOAE amplitude[a]				*DPOAE amplitude progression/5 days*[b]				*P65 DPOAE amplitude*[c]			
Hz	*−/−*	*+/− +/+*	*F (df, df)*	*p value*	*−/− (p value)*	*+/− +/+ (p value)*	*F (df, df)*	*p value*	*−/−*	*+/− +/+*	*F (df, df)*	*p value*
10,641	27.2	28.9	4.01 (1, 56)	0.0500	0.196 (0.0960)	0.306 (0.0003)**	0.58 (1, 500)	0.4478	29.0	31.6	10.34 (1, 56)	0.0022**
9,797	29.5	32.2	13.28 (1, 56)	0.0006**	0.062 (0.5514)	0.246 (0.0011)**	2.05 (1, 500)	0.1528	30.1	34.4	35.21 (1, 56)	<0.0001**
8,953	28.7	31.8	16.42 (1, 56)	0.0002**	0.080 (0.4479)	0.276 (0.0003)**	2.25 (1, 500)	0.1344	29.4	34.3	40.64 (1, 56)	<0.0001**
8,203	22.8	28.9	32.14 (1, 56)	<0.0001**	0.219 (0.0834)	0.297 (0.0012)**	0.25 (1, 500)	0.6187	24.7	30.6	41.68 (1, 56)	<0.0001**
7,547	19.3	21.8	2.43 (1, 56)	0.1250	−0.007 (0.9749)	0.497 (0.0047)**	2.87 (1, 500)	0.0908	19.2	26.3	19.61 (1, 56)	<0.0001**
6,891	7.6	15.1	34.99 (1, 56	<0.0001**	1.179 (<0.0001)**	1.083 (<0.0001)**	0.19 (1, 500)	0.6625	18.3	24.8	27.43 (1, 56)	<0.0001**
6,328	1.0	9.8	44.05 (1, 56)	<0.0001**	1.535 (<0.0001)**	1.354 (<0.0001)**	0.61 (1, 500)	0.4369	14.8	22.0	29.43 (1, 56)	<0.0001**
5,813	−6.5	3.8	57.22 (1, 56)	<0.0001**	1.478 (<0.0001)**	1.264 (<0.0001)**	0.83 (1, 500)	0.3615	6.8	15.1	37.85 (1, 56)	<0.0001**
5,297	−12.7	−2.1	67.73 (1, 56)	<0.0001)**	1.300 (<0.0001)**	1.265 (<0.0001)**	0.02 (1, 500)	0.8750	−1.0	9.3	64.00 (1, 56)	<0.0001**

df, df degrees of freedom numerator, degrees of freedom denominator

*p<0.05, significant level; **p<0.01, significant level

[a]Estimates of DPOAE amplitude by frequency for *Npc1*^{nih} homozygous (−/−) and control (+/−, +,+) animals at P20, and the effect of disease (genotype) at that point in time

[b]Estimates of progression in DPOAE amplitude for *Npc1*^{nih} homozygous (−/−) and control (+/−, + +) animals per 5-day test session; positive values denote an increase and negative values a decrease in DPOAE amplitude every 5 days, suggesting increased or diminished cochlear outer hair cell function, respectively. Statistical results examining the significance of genotype on progression within genotype (first two columns) and the significance of genotype on progression of DPOAE amplitude (last two columns) are shown

[c]Estimates of DPOAE amplitude for *Npc1*^{nih} homozygous (−/−) and control (+/−, +,+) animals at P65 and the effect of disease at that point in time

TABLE 2

Results of repeated measures modeling for ABR latency (ms) at P20 and P65 and ABR latency progression data (ms) for click stimuli

	P20 latency				*Latency progression/5 days*				*P65 latency*			
Click	*−/−*	*+/− +/+*	*F (df, df)*	*p value*	*−/− (p value)*	*+/− +/+ (p value)*	*F (df, df)*	*p value*	*−/−*	*+/− +/+*	*F (df, df)*	*p value*
I	1.37	1.37	0.16 (1, 56)	0.6918	0.005 (0.0159)*	−0.004 (0.0055)**	12.93 (1, 493)	0.8004	1.42	1.33	41.00 (1, 56)	<0.0001**
II	2.14	2.20	2.07 (1, 56)	0.1562	−0.003 (0.6334)	−0.030 (<0.0001)**	14.27 (1, 493)	0.0002**	2.11	1.91	23.32 (1, 56)	<0.0001**
III	3.23	3.17	0.94 (1, 56)	0.3360	−0.000 (0.9679)	−0.022 (0.0024)**	3.08 (1, 492)	0.0797	3.23	2.97	15.16 (1, 56)	0.0003**
IV	4.21	4.18	0.22 (1, 56)	0.6408	0.0003 (0.9743)	−0.039 (<0.0001)**	9.79 (1, 493)	0.0019**	4.21	3.83	33.27 (1, 56)	<0.0001**
V	5.10	5.02	0.97 (1, 56)	0.3289	−0.008 (0.5299)	−0.064 (<0.0001)**	14.32 (1, 493)	0.0002**	5.03	4.44	53.89 (1, 56)	<0.0001**
I–III	1.86	1.80	0.81 (1, 56)	0.3171	−0.005 (0.5575)	−0.017 (0.0105)*	1.06 (1, 492)	0.3039	1.81	1.64	6.89 (1, 56)	<0.0001**
III–V	1.87	1.83	0.28 (1, 56)	0.6340	−0.008 (0.4806)	−0.040 (<0.0001)**	5.92 (1, 492)	0.0153*	1.80	1.47	21.74 (1, 56)	<0.0001**
I–V	3.73	3.65	0.96 (1, 56)	0.3310	−0.012 (0.2593)	−0.059 (<0.0001)**	10.54 (1, 493)	0.0012**	3.61	3.12	41.58 (1, 56)	<0.0001**

See Table 1 for a detailed description of table formatting

*$p<0.05$, significant level; **$p<0.01$ significant level

df, df degrees of freedom numerator, degrees of freedom denominator

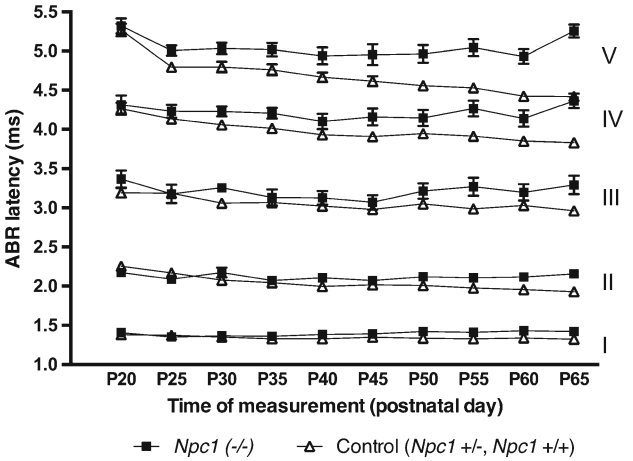

FIG. 4. Mean (SEM) ABR latency data for *Npc1^{nih}* homozygous mutant (−/−) and control (+/−, +/+) mice across the experimental lifetime for component waves I–V.

the spiral ganglion cells, suggesting the material identified within inclusion bodies by light-level imaging is not unesterfied cholesterol but, most likely, ganglioside (Walkley and Suzuki 2004).

Transmission electron microscopy was used to further describe the morphology of the various inclusion bodies identified by light microscopic imaging. The lysosomal accumulations seen in the supporting cells of the organ of Corti strongly resemble those found in the intermediate cells of the stria vascularis (Fig. 7) and correspond in location to the unesterfied cholesterol identified by filipin staining. However, the accumulations seen in the spiral ganglion appear to differ and, therefore, are unlikely to be unesterified cholesterol. Swollen nerve endings found in the organ of Corti appear to be filled with cellular debris.

DISCUSSION

We present data that, for the first time, identify hearing loss in a common mouse model for NPC1 disease. BALB/c-*Npc1^{nih}* homozygous mutant mice exhibited elevation in high-frequency ABR thresholds as early as P20, which is weeks before diseased mice show deficits in the acoustic startle (Maue et al. 2011) or overtly display neurologic impairment (e.g., ataxia, tremor, and dystonia). This finding was completely penetrant across mutant offspring within the first 3 weeks of life, which suggests early deterioration, maturational dysfunction, or both within the auditory system.

Our histological observations revealed cellular changes in cochlear tissues and peripheral auditory nerve. Filipin staining demonstrated abnormal lysosomal cholesterol accumulation in cells of the organ of Corti and stria vascularis, which both contribute to

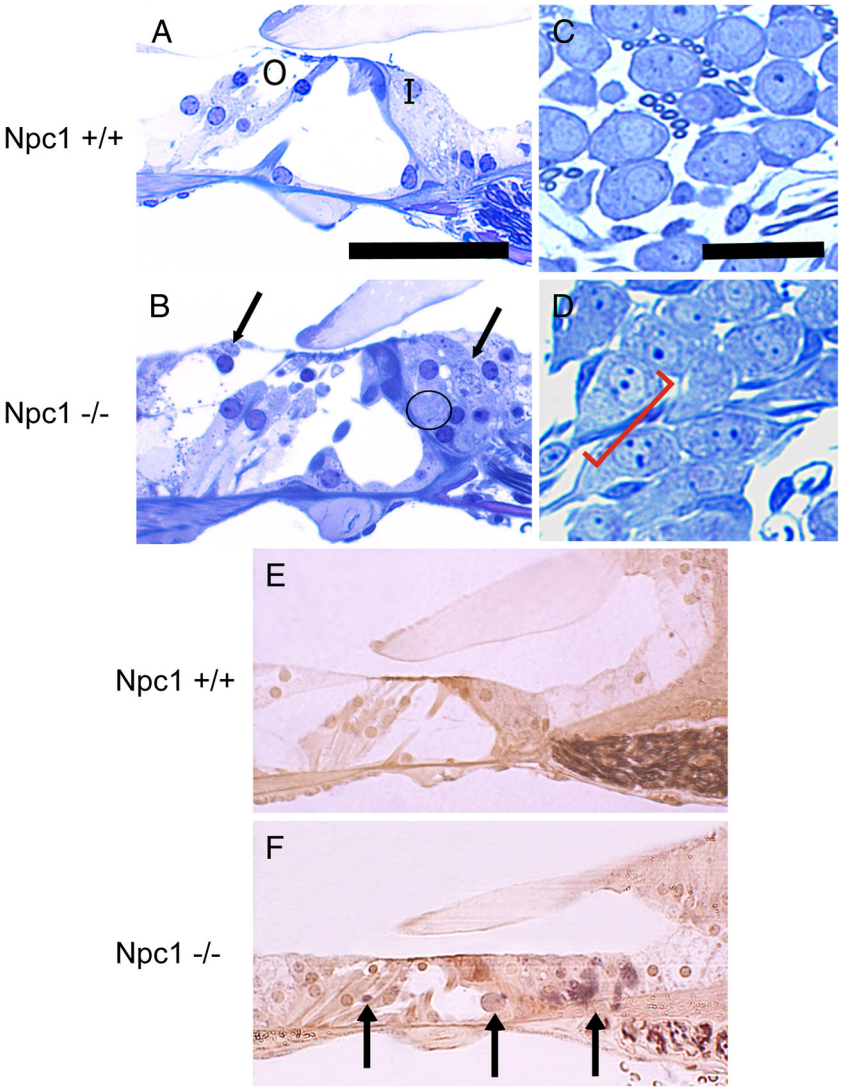

FIG. 5. **A–D** Light micrographs of the organ of Corti and spiral ganglion from Embed 812-embedded tissues sectioned at 5 µm and stained with toluidine blue from P70 *Npc1*^{nih} homozygous mutant (Npc1 −/−) and control (Npc1 +/+) mice. Inner (*I*) and outer (*O*) hair cells are denoted in control image (**A**). In (**B**), *circle* surrounds swollen nerve fibers and *small arrows* point to granular material within cells, which were not observed in Npc1 +/+mice (**A**). In the basal-turn spiral ganglia (**C**, **D**) cell bodies in *Npc1*^{nih} homozygous mutant (Npc1 −/−) mice (D) exhibit expansion/elongation of the cell body at the poles. The red bracket identifies the major axis of such an elongated cell in (**D**). *Bar* in (**A**)=50 µm; bar in (**C**)=20 µm. **E**, **F** Light micrographs of thick-sectioned (approximately 30 µm); Embed 812-processed organs of Corti from the basal turn of P30 *Npc1*^{nih} homozygous control (Npc1 +/+, **E**) and mutant (Npc1 −/−, **F**) mice. Toluidine blue stain was not used on these sections to better visualize the dark gray, osmium-stained swellings of the nerve fibers in the inner hair cell region, the tunnel of Corti, and below the outer hair cells in Npc1 −/− samples (**F**, *arrows*).

the cochlear portion of hearing function. Abnormal accumulations of lysosomal material (possibly gangliosides) in the spiral ganglion cell body and swelling of nerve endings within the organ of Corti indicate damage to the neural tissue as well.

The significantly smaller DPOAE amplitudes in *Npc1*^{nih} homozygous mutant mice compared with controls (+/−, +/+) indicate less robust cochlear outer hair cell function and support a cochlear contribution to the hearing loss at P20. The increase in DPOAE amplitude in *Npc1*^{nih} control (+/−, +/+) animals observed across the experimental lifespan suggests postnatal cochlear maturation through at least P65 in this BALB/c background strain. These changes in amplitude were larger for lower frequencies (<7 kHz) and similar to those observed in C57BL/6J mice (Narui et al 2009). This suggests the basal region of the cochlea may be more developmentally mature in the BALB/c background strain, and that regions more apical undergo postnatal developmental changes in the mechanical properties of the basilar membrane or the electromotility of the outer hair cells (Long and Tubis 1988; Brown et al. 1989) or stereocilia bundle (Liberman et al. 2004). As differences in DPOAE development were observed between *Npc1*^{nih} homozygous mutant mice and controls (+/−, +/+), and as NPC1 has no known or predicted effects on middle ear physiology, it is reasonable to hypothesize that the observed effects on DPOAE amplitude in the current study are based on changing properties of the developing cochlea and that NPC1 pathogenesis may disrupt maturational processes or accelerate age-related changes in mice.

By P65, homozygous mutant *Npc1*^{nih} mice had significantly longer latencies for the component peaks of the ABR waveform compared with control (+/−, +/+) animals, which did not correlate with the neurodegenerative phenotype in the mutants, but, rather, reflected a significant shortening in latency for control animals. To the best of our knowledge, developmental changes in

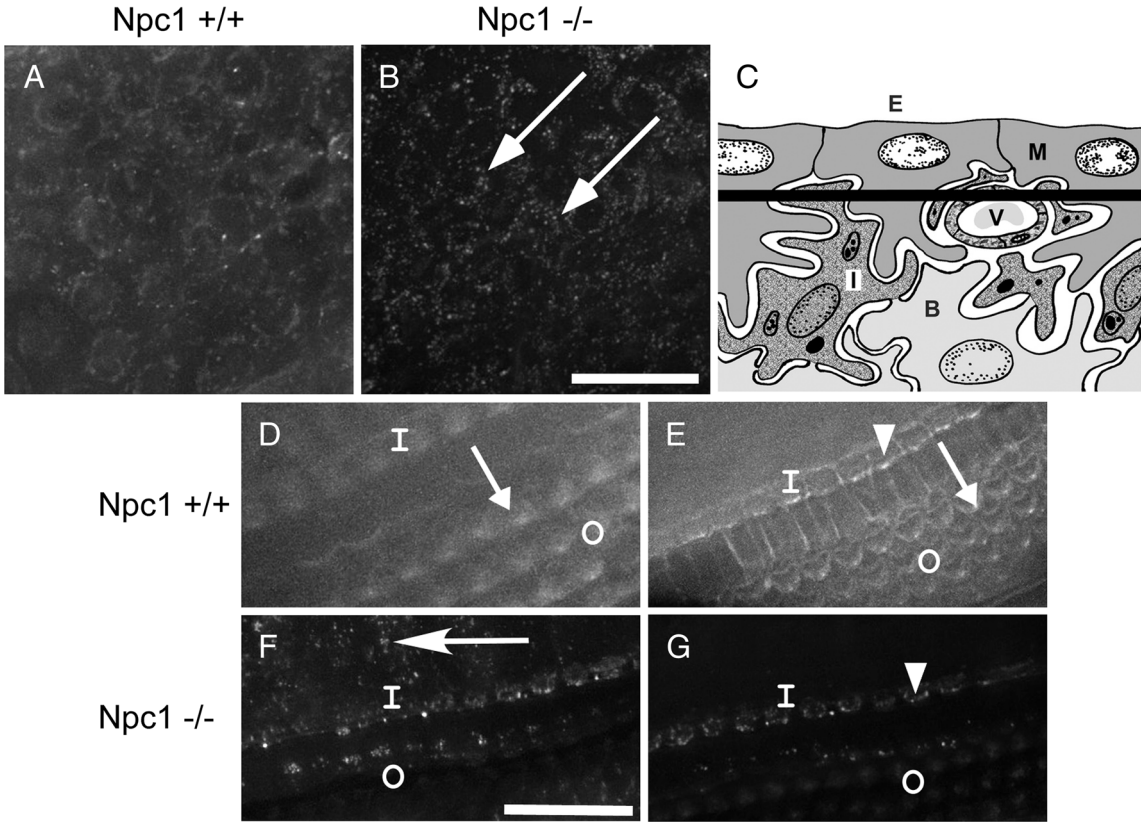

FIG. 6. **A**–**G** Filipin-stained fluorescence images of stria vascularis (**A**, **B**, *bar*=25 μm) and organ of Corti (**D**–**G**, *bar*=25 μm) from P50 *Npc1*^{nih} homozygous mutant (Npc1 −/−) and control (Npc1 +/+) mice. Z-stacks were deconvolved and maximum-intensity projected. Images from wild type and Npc1 −/− specimens in (**A**) and (**B**) are displayed on the same intensity scale. Punctate intracellular filipin staining observed in tissues of (Npc1 −/−) mice (**B**, **F**, **G**) is indicative of lysosomal unesterfied cholesterol accumulation, a hallmark characteristic of NPC-affected cells. Very little punctate staining was seen in (Npc1 +/+) mice (**A**, **D**, **E**). The focal volume in (**A**, **B**) is depicted diagramatically in (**C**) looking into the stria vascularis from the endolymphatic surface; *E* endolymph, *M* marginal cell, *I* intermediate cell, *B* basal cell, *V* vessel. Punctate staining in (**B**) was especially prominent within the intermediate cell layer. **D**, **F** Images are focused at the hair cell base; **E**, **G** images are focused at the cuticular plate. **D** Image has been rotated 20 ° clockwise to match the orientation of image (**E**), which was taken from a different Z-stack. **F**, **G** Images were taken from the top and bottom half of the same Z-stack. They were rotated 94 ° counterclockwise for easier comparison with (**D**) and (**E**). Filipin-labeled inner hair cell stereocilia (**E**, **G**, *arrowhead*) and outer hair cell fonticulus (**D**, **E**, *arrow*) can be observed. The *arrow* in (**F**) points to large accumulations of lysosomal cholesterol in the inner sulcus and/or inner border cells. *I* inner hair cell, *O* outer hair cell regions.

ABR latency in mice have not been reported previously, although similar changes have been well documented in other mammals, including humans (Hecox and Galambos 1974). While initial detection and saturation of the ABR (threshold) has been reported in C57BL/6J mice (Lenoir and Puel 1987), our data provide a more detailed depiction of postnatal maturation of the ABR in the BALB/c background strain. Almost every component peak of the ABR exhibited significant progressive shortening with age in control animals, and the effect was larger for later-occurring peaks. A similar maturational effect was observed for ABR amplitude, where all mice demonstrated a significant decrease in waveform amplitude across the experimental lifespan (data not shown). This postnatal change in ABR latency and amplitude did not occur in *Npc1*^{nih} homozygous mutant mice, thus providing further support for disease-related maturational disruption. We cannot rule out the additional possibility, however, that normal maturation in mutant animals is masked by concurrent degeneration within the auditory system.

Auditory brainstem histopathology has been localized to the cochlear nucleus, inferior colliculus, and medial geniculate nucleus of *Npc1*^{nih} mutant animals (Luan et al. 2008), which corresponds to our data that indicate dysfunctional neural activity in *Npc1*^{nih} mutant mice underlying the later component peaks of the ABR (e.g., wave V). Prolongation in later waves (e.g., wave V) and interpeak latencies (e.g., III–V) of the ABR cannot be explained by cochlear hearing loss alone and reflect delay in transmission time through the auditory brainstem.

The relationship between over-accumulation of cholesterol and hearing has been examined, but remains unclear. In humans, inconclusive evidence suggests a correlation between hyperlipidemia and

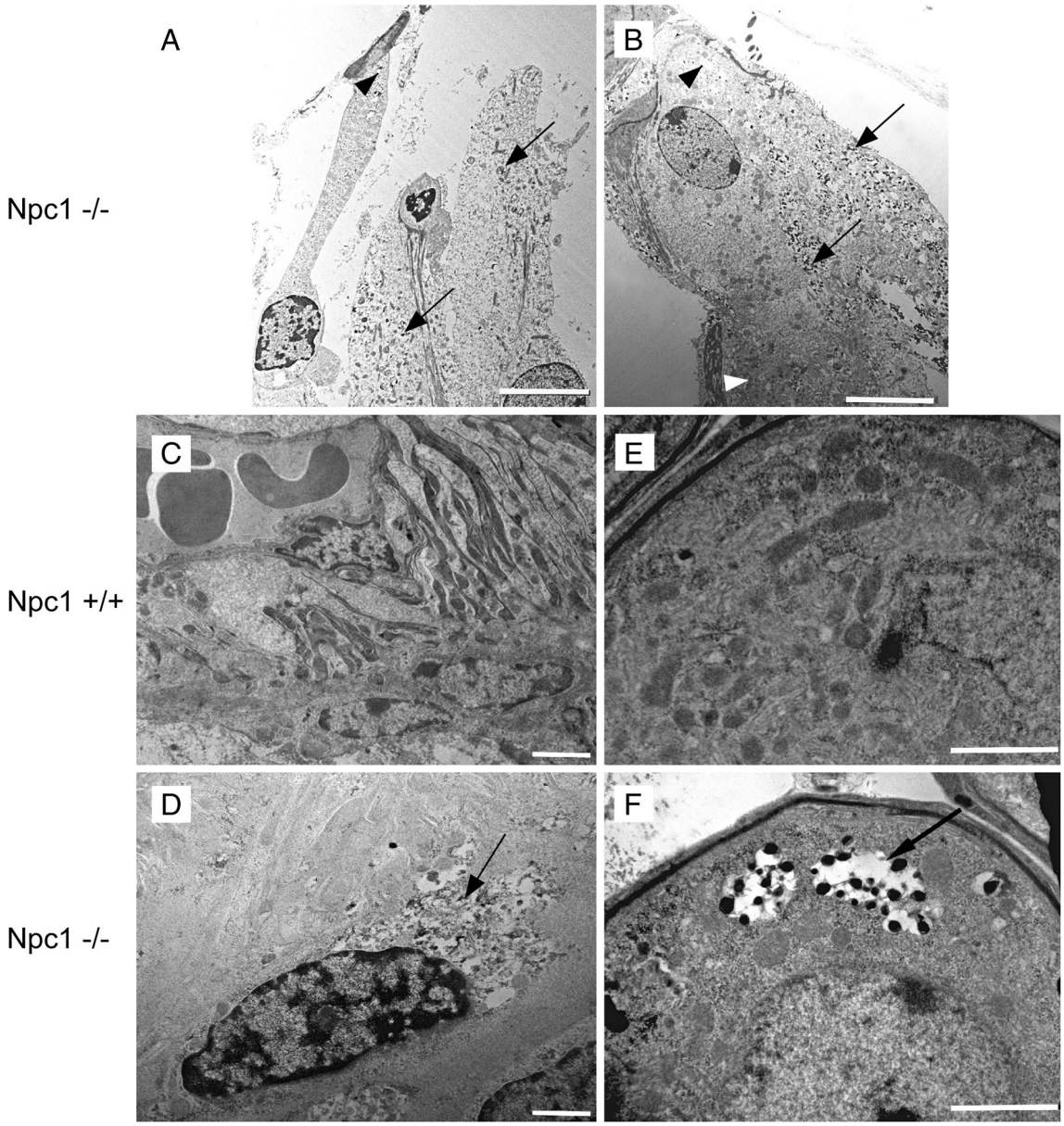

FIG. 7. Electron micrographs of hair cells from P30 *Npc1*^{nih} homozygous mutant (Npc1 −/−) mice (**A**, **B**, *bar*=3 μm) and stria vascularis (**C**, **D**) and myelinated spiral ganglion cells from P70 (**E**, **F**) *Npc1*^{nih} homozygous mutant (Npc1 −/−, **D**, **F**) and control (Npc1 +/+, **C**, **E**) mice. **C**, **D** Images were taken at the level of the vessel and intermediate cell (*I*) in the diagram (Fig. 6G). All images are from the basal area of the cochlea. Dark inclusion bodies (*arrows*) can be seen in the supporting cells of both the outer hair cell region (**A**) and inner hair cell region (**B**) of the organ of Corti, with less evidence of inclusion bodies in the hair cells themselves (*arrowheads* in **A**, **B**). Similar material is seen in the intermediate cells of the stria vascularis from the mutant mice (**D**, *arrow*). Material seen in the inclusions within the spiral ganglion cell bodies (**F**, *arrow*), appeared very dense, compact, and whorled.

sensorineural hearing loss (Evans et al. 2006; Preyer et al. 2001), with speculation that the effect may be greater at the cochlear basal turn and corresponding high frequency test region where the cochlea is more susceptible to ischemic change (Cunningham and Goetzinger 1974). Deleterious effects of hyperlipidemia on hearing and cochlear morphology have been shown in mice (Guo et al. 2005) and guinea pigs, which, collectively, support a complex role for cholesterol and other lipids in the auditory system. Systemic effects of hyperlipidemia, however, may affect the ear differently than localized accumulation of unesterfied cholesterol seen in NPC1.

Within the cochlea, cholesterol regulates lipid composition, mobility, and stiffness of the lateral walls of the outer hair cells (Evans et al. 2006). Changes in cochlear cholesterol levels can modulate the amplitude of DPOAEs in mice, highlighting the intimate relationship between cholesterol in the outer hair cell wall and the membrane protein prestin that regulates

motility and tuning of the cochlear outer hair cells. Levels of membrane cholesterol decrease during maturation of the cochlear outer hair cells, which may help tune these sensory cells to function maximally (Rajagopalan et al. 2007). Cholesterol has also been identified as a critical component in determining the magnitude of voltage-gated potassium currents within developing (Levic and Yamoah 2011) and postnatal (Purcell et al. 2011) cochlear hair cells.

The critical role of cholesterol in developing cochlear hair cells may explain why DPOAEs from homozygous mutant *Npc1*^{nih} mice in the current study did not achieve levels consistent with their control littermates during maturation. We speculate that disease-related alterations in the processing of cellular cholesterol prohibit the natural reduction in cholesterol necessary for cochlear cells to mature completely. As unesterified cholesterol, sphingolipids, and gangliosides accrue within cells throughout the disease process, further detrimental effects on cellular structure and function are likely, and may manifest as progressive declines in auditory function. This hypothesis applies to both cochlear cells, and areas of neural tissue with high concentrations of lipids, including the myelinated auditory nerve, accounting for both the cochlear and neural dysfunction we observed in *Npc1*^{nih} homozygous mutant animals. Furthermore, these data may reflect an association between *Npc1* pathogenesis and an accelerated onset of age-related deterioration in the inner ear and neural auditory pathway. Additional histological studies, evaluation of serum cholesterol levels in the cochlea, and novel research exploring the role of cholesterol in the auditory system of the developing *Npc1*^{nih} mouse are necessary to explore these theories.

Recent auditory data from humans with NPC1 (King et al. 2014) support the presence of auditory dysfunction in most patients with the disease. Despite a heterogeneous sample, functionally significant high frequency hearing loss was observed in over half of the cohort and the hearing loss was progressive in a subset of patients followed longitudinally. The presentation in the majority (66 %) of individuals was consistent with a neural site of lesion involving the auditory nerve and auditory brainstem pathways, although cochlear involvement was also evident. The findings herein are consistent with those reported in humans with NPC1, although not entirely parallel. Other mouse models of NPC1 (Npc1^{nmf164}) have a less severe neurological presentation than the *Npc1*^{nih} mouse (Maue et al. 2011), and it will be useful to extend the examination of genotype–phenotype differences to auditory function in these models. Understanding how the auditory system is affected in both a heterogeneous human population and inbred homogenous animal models like the *Npc1*^{nih} mouse has important implications when considering markers for disease status, progression, and future therapeutic safety and efficacy.

ACKNOWLEDGMENTS

This work was supported by intramural research funds Z01 DC 000060 and Z01 DC 000064 of the National Institute on Deafness and Other Communication Disorders and the Eunice Kennedy Shriver National Institute of Child Health and Human Development, National Institutes of Health (to AJG, FDP, CCB) and the Ara Parseghian Medical Research Foundation (to JJR). Further support came from training grants from the National Institute on Deafness and Other Communication Disorders (T32DC000046 supporting KAK), and the National Institute of General Medical Sciences (T32GM007062 supporting AMT) of the National Institutes of Health. The authors would like to acknowledge the assistance of Katherine Luby-Phelps (Director) and the UT Southwestern Live Cell Imaging Facility, a Shared Resource of the Harold C. Simmons Cancer Center, supported in part by an NCI Cancer Center Support Grant, 1P30 CA142543-01. The authors are grateful to Robert Dooling, Tracy Fitzgerald, Arthur Popper, and Thomas Friedman for their insightful feedback on methodology and careful review of the manuscript. Thanks to Suzanne Lenhard and Elena Koulich for technical assistance and to the veterinary staff at NIDCD who provided exceptional support, most notably Pat Diers, Donny Catts, and James McGehee.

REFERENCES

Brown AM, McDowell B, Forge A (1989) Acoustic distortion products can be used to monitor effects of chronic gentamicin treatment. Hear Res 42:143–156

Crowder MJ, Hand DJ (1990) Analysis of repeated measures. Chapman and Hall, New York

Cunningham DR, Goetzinger CP (1974) Extra-high frequency hearing loss and hyperlipidemia. Audiology 13:470–484

Evans MB, Tonini R, Do Shope C, Oghalai JS, Jerger JF, Insull W, Brownell WE (2006) Dyslipidemia and auditory function. Otol Neurotol 27:609–614

Fink JK, Filling-Katz MR, Sokol J, Cogan DG, Pikus A, Sonies B, Soong B, Pentchev PG, Comly ME, Brady RO et al (1989) Clinical spectrum of Niemann–Pick disease type C. Neurology 39:1040–1049

Garver WS, Francis GA, Jelinek D, Shepherd G, Flynn J, Castro G, Walsh Vockley C, Coppock DL, Pettit KM, Heidenreich RA et al (2007) The National Niemann–Pick C1 disease database: report of clinical features and health problems. Am J Med Genet A 143:1204–1211

German DC, Quintero EM, Liang CL, Ng B, Punia S, Xie C, Dietschy JM (2001) Selective neurodegeneration, without neurofibrillary tangles, in a mouse model of Niemann–Pick C disease. J Comp Neurol 433:415–425

Guo Y, Zhang C, Du C, Nair U, Yoo T (2005) Morphological and functional alterations of the cochlea in apolipoprotein E gene deficient mice. Hear Res 208:54–67

Hecox K, Galambos R (1974) Brain stem auditory evoked responses in human infants and adults. Arch Otolaryngol 99:30–33

Institute for Laboratory Animal Research, Committee for the Update of the Guide for the Care and Use of Laboratory Animals (2011) Guide for the Care and Use of Laboratory Animals, Eighth Edition. National Research Council of the National Academies

King KA, Gordon-Salant S, Yanjanin N, Zalewski C, Houser A, Porter FD, Brewer CC (2014) Auditory phenotype of Niemann–Pick disease, type C1. Ear Hearing 35:110–117

Lenoir M, Puel JL (1987) Development of 2*f*1–*f*2 otoacoustic emissions in the rat. Hear Res 29:265–271

Levic S, Yamoah E (2011) Plasticity in membrane cholesterol contributes toward electrical maturation of hearing. J Biol Chem 7:5768–5773

Li H, Repa JJ, Valasek MA, Beltroy EP, Turley SD, German DC, Dietschy JM (2005) Molecular, anatomical, and biochemical events associated with neurodegeneration in mice with Niemann–Pick type C disease. J Neuropathol Exp Neurol 64:323–333

Liberman MC, Zuo J, Guinan JJ Jr (2004) Otoacoustic emissions without somatic motility: can stereocilia mechanics drive the mammalian cochlea? J Acoust Soc Am 116:1649–1655

Liscum L, Faust JR (1987) Low density lipoprotein (LDL)-mediated suppression of cholesterol synthesis and LDL uptake is defective in Niemann–Pick type C fibroblasts. J Biol Chem 262:17002–17008

Liscum L, Ruggiero RM, Faust JR (1989) The intracellular transport of low density lipoprotein-derived cholesterol is defective in Niemann–Pick type C fibroblasts. J Cell Biol 108:1625–1636

Loftus SK, Morris JA, Carstea ED, Gu JZ, Cummings C, Brown A, Ellison J, Ohno K, Rosenfeld MA, Tagle DA et al (1997) Murine model of Niemann–Pick C disease: mutation in a cholesterol homeostasis gene. Science 277:232–235

Long GR, Tubis A (1988) Investigations into the nature of the association between threshold microstructure and otoacoustic emissions. Hear Res 36:125–139

Luan Z, Saito Y, Miyata H, Ohama E, Ninomiya H, Ohno K (2008) Brainstem neuropathology in a mouse model of Niemann–Pick disease type C. J Neurol Sci 268:108–116

Maue RA, Burgess RW, Wang B, Wooley CM, Seburn KL, Vanier MT, Rogers MA, Change CC, Chang TY, Harris BT et al (2011) A novel mouse model of Niemann–Pick type C disease carrying a D1005G-Npc1 mutation comparable to commonly observed human mutations. Hum Mol Genet 21:730–750

Narui Y, Minekawa A, Iizuka T, Furukawa M, Kusunoki T, Koike T, Ikeda K (2009) Development of distortion product otoacoustic emission in C57BL/6 J mice. Int J Audiol 48:576–581

Ong WY, Kumar U, Switzer RC, Sidhu A, Suresh G, Hu CY, Patel SC (2001) Neurodegeneration in Niemann–Pick type C disease mice. Exp Brain Res 141:218–231

Ordonez MP, Roberts EA, Kidwell CU, Yuan SH, Plaisted WC, Goldstein LSB (2012) Disruption and therapeutic rescue of autophagy in a human neuronal model of Niemann Pick type C1. Hum Mol Genet 21:2651–2662. doi:10.1093/hmg/dds090

Ory DS (2000) Niemann–Pick type C: a disorder of cellular cholesterol trafficking. Biochim Biophys Acta 1529:331–339

Patterson MC, Vanier MT, Suzuki K, Morris JA, Carstea ED, Neufeld EB, Blanchette-Mackie JE, Pentchev PG (2001) Niemann–Pick disease type C: a lipid trafficking disorder. In: Scriver CR (ed) The metabolic and molecular bases of inherited disease. McGraw-Hill, New York, pp 3611–3633

Pikus A (1991) Audiologic profile in Niemann–Pick C. Ann N Y Acad Sci 630:313–314

Preyer S, Baisch A, Bless D, Gummer AW (2001) Distortion product otoacoustic emissions in human hypercholesterolemia. Hear Res 152:139–151

Purcell EK, Liu L, Thomas PV, Duncan RK (2011) Cholesterol influences voltage-gated calcium channels and BK-type potassium channels in auditory hair cells. PLoS ONE 6(10):e26289. doi:10.1371/journal.pone.0026289

Rajagopalan L, Greeson JN, Xia A, Liu H, Sturm A, Raphael RM, Davidson AL, Oghalai JS, Pereira FA, Brownell WE (2007) Tuning of the outer hair cell motor by membrane cholesterol. J Biol Chem 282:36659–36670

Vincent I, Bu B, Erickson RP (2003) Understanding Niemann–Pick type C disease: a fat problem. Curr Opin Neurol 16:155–161

Võikar V, Rauvala H, Ikonen E (2002) Cognitive deficit and development of motor impairment in a mouse model of Niemann–Pick type C disease. Behav Brain Res 132:1–10

Walkley S, Suzuki K (2004) Consequences of NPC1 and NPC2 loss of function in mammalian neurons. Biochem et Biophys Acta 1685:48–62

Ward S, O'Donnell P, Fernandez S, Vite CH (2010) 2-hydroxypropyl-ß-cyclodextrin raises hearing threshold in normal cats and in cats with Niemann–Pick type C disease. Pediatr Res 68:52–56

Weintraub H, Abramovici A, Amichai D, Eldar T, Ben-Dor L, Pentchev PG, Hammel I (1992) Morphometric studies of pancreatic acinar granule formation in NCTR-Balb/c mice. J Cell Sci 102(Pt 1):141–147

Willott JF, Turner JG, Carlson S, Ding D, Bross LS, Falls WM (1998) The BALB/c mouse as an animal model for progressive sensorineural hearing loss. Hear Res 115:162–174